Optical manipulation and study of single gold nanoparticles in solution

Ruijgrok, P.V.

3

Optical trapping apparatus, and characterization of optical trapping of single gold nanorods

3.1 Introduction

In this chapter we discuss the optical trapping apparatus that was built during this project. We demonstrate the capabilities of the setup by a detailed characterization of the optical trapping of single gold nanorods. We will discuss the experimental methods used to characterize the optical trap, to characterize the trapping of a single particle as well as detect the presence of multiple particles in the trap. We record the white-light scattering spectrum of each individual trapped rod to measure its aspect ratio, and study the thermal stability of the rods. We show that the nanorods align with the polarization of the trap laser by measuring the polarization and spectrum of the scattering light. Using scattering correlation spectroscopy we record both the translational and rotational fluctuations of the trapped rod to characterize the orientational and translational trap stiffnesses.

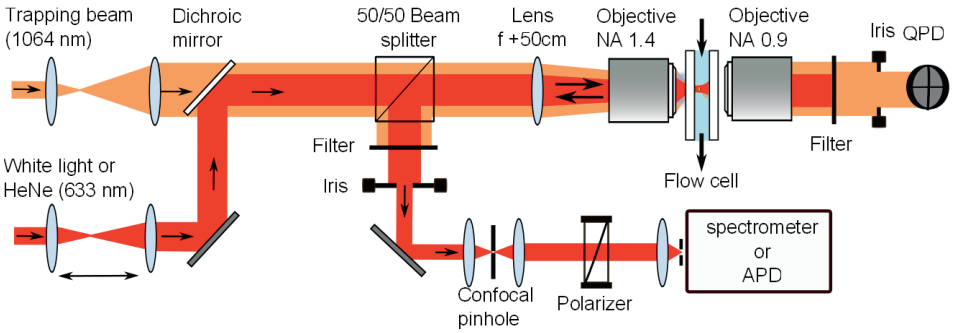

Figure 3.1: a) Scheme of the optical trap. QPD, Quadrant photodiode; APD, Avalanche photodiode

3.2 Methods and materials

3.2.1 Optical trapping setup, and integration with other microscopies

The optical setup schematically shown in Fig 3.1 consists of a single-beam optical trap at 1064 nm (5W IPG Photonics Ytterbium fiber laser). The home-built optical microscope was constructed during this project and has its optical axis parallel to the plane of the optical table (horizontal). The horizontal beam-axis facilitates the integration of the several optical setups that were used in the experiments described in this thesis. The microscope design (shown in Appendix B) aimed at optimizing mechanical and thermal stability.

The trapping beam is focused into water about 25 μm away from the glass substrate by an objective with a high numerical aperture (Olympus oil immersion 60 x, 1.4 NA). To alleviate the spherical aberrations introduced by water's too low index, the incoming trapping beam was made slightly convergent by means of a 50 cm lens just before the objective.[118] This abberation correction was essential to achieve stable trapping of gold nanoparticles.

To obtain scattering spectra, white light from a Xenon arc lamp was focused to a spot and overlapped with the trap focus. Scattered light was collected by the focusing objective and detected by a nitrogen-cooled CCD camera coupled to a spectrograph. An iris inserted into the detection path selected the center 5 mm of the beam, to minimize depolarization effects by the objective. We inserted a 50 μm confocal pinhole at the focus of a 10 cm lens to reduce the background.

Translation and rotation dynamics of the trapped rods were deduced from

the back-scattered light of a HeNe laser (633 nm), detected by a single-photon counting photodiode (Perkin Elmer) and analyzed with a correlation card (PicoQuant). For the experiment we used a function generator to provide a reference signal with a frequency of 10 MHz. In all experiments, count rates at the detector were in the range $2 \cdot 10^5 - 4 \cdot 10^5$ counts per second.

3.2.2 Materials

Gold nanorods with 60 nm average length and 25 nm average diameter (sample 25 nm$\times$60 nm) and with 92 nm average length and 33 nm average width (sample 30 nm$\times$90 nm) were synthesized by the silver-assisted seed-mediated method[119] in the presence of cetyltrimethylammonium bromide (CTAB) and coated with thiolated polyethyleneglycol (mPEG, MW5000, Sigma Aldrich) to prevent their aggregation in pure water.[120] The rod suspensions were diluted with ultrapure water to limit the trapping of multiple particles during the course of a measurement, up to 2 hours.

3.2.3 Calibration of effective numerical aperture and intensity at the trap focus

An important technical factor is the calibration of the intensity at the trap focus. The actual intensity at the trap focus is considerably reduced compared to the intensity that could be calculated in the ideal case for the following reasons: i) the objective's transmission in the NIR is only 19 %; ii) the objective is not corrected for imaging in water. Spherical aberrations reduce the intensity at the focus; iii) because of total internal reflection at the glass-water interface, the effective numerical aperture at the focus cannot exceed the index of refraction of water. Indeed, it is significantly weaker than 1.4, as explained hereafter.

The plot of Fig. 3.2 has been obtained by placing an iris on the NIR beam in front of the lens-objective system of the trap. The rotational correlation rate (inverse of the rotational correlation time), which is directly proportional to the local intensity at the focus (see Sec. 3.7) has been measured as a function of the beam diameter corresponding to the iris aperture (due to the convergence of the beam introduced by the lens, the diameter of the beam at the objective back aperture is about 0.8 times the iris aperture). We see that the trapping strength increases steeply with beam diameter, both because the transmitted power increases and because the numerical aperture increases. The measurements are in qualitative agreement with a function scaling as a

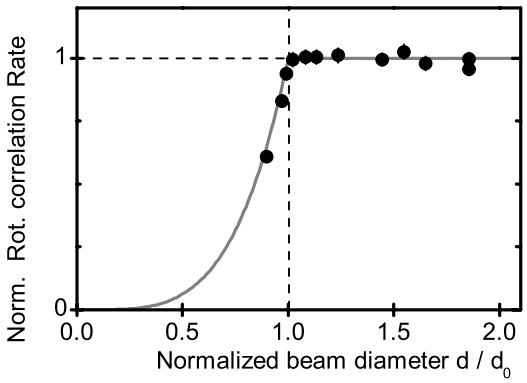

Figure 3.2: Determination of the effective numerical aperture of the trapping beam by the local intensity at the focus. The rotational correlation rate (inverse of the rotational correlation time), measured on a single trapped nanorod (25 nm $\times$60 nm sample), is proportional to the local intensity. The measurements are plotted as function of the normalized beam d/d_0, where d_0 is 8 mm at the objective back aperture, and the objective back aperture is 11.5 mm in diameter. The solid line is a concatenation of the functions $f(d) = (d/d_0)^4$ for $d < d_0$ and $f(d) =$ constant for $d > d_0$.

beam diameter to the fourth power, expected for this situation. For a beam diameter above a characteristic diameter d_0, the local intensity at the focus remains constant. That means that the off-axis rays do not contribute to trapping. The numerical aperture corresponding to this characteristic diameter is 1.0 and has been used as the effective NA at the trap focus.

3.2.4 Identification of single and multiple trapped nanorods by their white light scattering spectra

To identify nanorods in the optical trap we have recorded their white light scattering spectrum. Our current procedure to trap a single rod is to start from a rather diluted suspension, and to wait for one nanorod to get trapped. At low enough concentration, this waiting time is about 10 minutes. The concentration of diffusing rods continuously decreases with time because rods stick to the surfaces of the flow cell. Therefore, trapping a second rod becomes more and more unlikely as time goes. Nonetheless, it occasionally happens. In that case, we observe a stepwise increase in scattered intensity, and the spectrum often clearly shows a split or broadened shape, as illustrated in Fig. 3.3. Usually, one of the two trapped rods is quickly ejected from the trap (after a few minutes) and either the initial rod or the newcomer re-

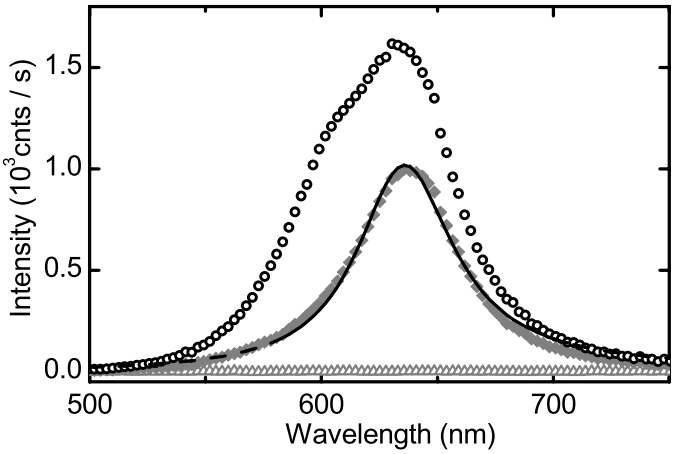

Figure 3.3: Spectra of scattered white light when zero (open gray triangles), one (solid gray diamonds) or two nanorods (open black circles) are trapped. Note the broadened and asymmetric shape of the latter spectrum due to difference in shape and size of the two trapped rods (sample: 25 nm $\times$ 60 nm). The spectrum changes in a stepwise way, as a new rod enters of leaves the trap. The black line is a Lorentzian fit (on an energy scale), where the fitted region is indicated by the solid part of the line. The width of the single particle spectrum is 50 nm (0.155 eV), a typical width of the plasmon resonance under our conditions.

mains in the trap for a long time. Trapping more than two rods only happens at high concentrations. In all measurements reported here there was only one nanorod in the trap.

3.3 Theory of optical forces and torques on gold nanorods

In this chapter we demonstrate the capabilities of our optical trapping setup by the stable three dimensional trapping of single gold nanorods. In this section we discuss the optical forces and torques acting on a gold nanorod in an optical field.

The optical response of a particle much smaller than the wavelength of light can be well described in the electrostatic limit, considering the particle as a dipole. The gold nanoparticles of sizes used in this thesis are small enough to be well described by this approximation. The scattering and absorption properties of the particle, and the optical forces and torques acting on the particle in the trap, can be calculated from the polarizability.

3.3.1 Polarizability

To evaluate the optical properties of the gold nanorods we calculate the polarizability of a prolate spheroid in the dipole approximation. For polarization of the incoming light parallel or perpendicular to the long principal axis of the ellipsoid, the polarizability is given as:[6]

$$\alpha_{\parallel,\perp}(\lambda) = 3\epsilon_0\epsilon_m(\lambda)V_p\frac{\epsilon(\lambda)-\epsilon_m(\lambda)}{3\epsilon_m(\lambda)+3L_{\parallel,\perp}\left[\epsilon(\lambda)-\epsilon_m(\lambda)\right]} \tag{3.1}$$

where V_p is the volume of the particle, ϵ_m and ϵ are the complex dielectric functions of the medium and gold respectively and $L_\parallel$ and $L_\perp$ are geometrical factors. $L_\parallel$ is given by

$$L_\parallel = \frac{1-e^2}{e^2}\left(-1+\frac{1}{2e}\ln\frac{1+e}{1-e}\right) \tag{3.2}$$

where e is the eccentricity, given as $e=\sqrt{1-\rho^2}$, with ρ the aspect ratio of the spheroid. For $L_\perp$, we have

$$L_\perp = \frac{1-L_\parallel}{2} \tag{3.3}$$

As the complex dielectric function of gold, we take the values measured by Johnson and Christy for bulk gold,[113] see Appendix C. In the calculation of the polarizability of the gold nanorods, this bulk complex dielectric function is modified to take into account additional damping mechanisms present in the nanoparticle, electron surface scattering and radiation damping.[121]

In order to match the spectral width of the calculated scattering spectrum to the spectrum observed in the experiment we incorporate a larger damping than the values that were reported in Novo *et al.*[121] We attribute this additional damping to chemical interface damping introduced by the thiol groups that bind the PEG capping layer to the gold.[122] Part of the broadening of the linewidth could also be introduced by the increased temperature of the gold nanorod in the trap, via electron-phonon coupling. This broadening is on the order of 0.1 meV /K,[123] contributing an increase in linewidth of only 7-8 meV at the highest trapping power. Therefore, the heating contribution to the linewidth is a minor effect. We will explore the temperature dependence of the plasmon damping further in Chapter 5.

Figure 3.4 displays the polarizability of a gold nanorod of dimensions typical in our experiment, calculated using the above expressions.

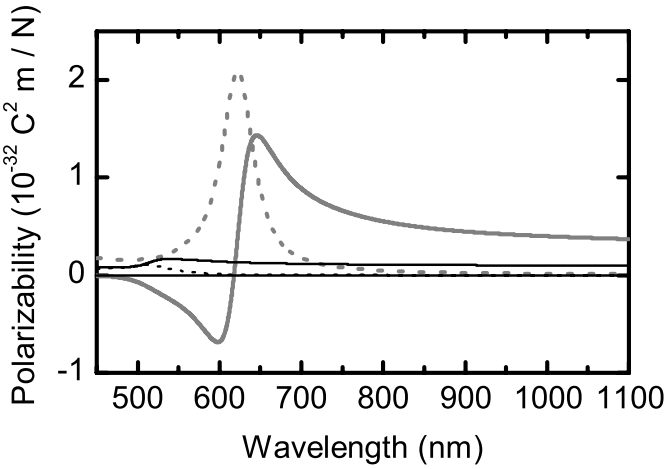

Figure 3.4: Calculated polarizability of a gold nanorod in water, in the dipole approximation (eqn 3.1). Grey (black) solid lines: real part of the polarizability for a field along the long axis (one of the short axes) of the rod. Gray (black) dashed lines: the imaginary part of the polarizability along the long axis (one of the short axes) of the rod. The nanorod has a volume $2.5 \cdot 10^4$ nm^3 and an aspect ratio of 2.45 .

3.3.2 Optical forces

The optical forces that act on the gold nanoparticle are the gradient force $\vec{F}_{\text{grad}}$ and the dissipative force $\vec{F}_{\text{d}}$ due to the radiation pressure of the absorbed photons. In the dipole approximation the scattering force vanishes.[124] The total force $\overrightarrow{F}$ on the particle is given as $\vec{F} = \vec{F}_{\text{grad}} + \vec{F}_{\text{d}}$. For an optical field $\vec{E}(\vec{r},t) = \text{Re}\left\{ \vec{E}_0(\vec{r}) \exp(-i\omega t) \right\}$, the time-averaged gradient force on a particle with polarizability α is given as[124]

$$\langle \vec{F}_{\text{grad}}(\vec{r}) \rangle = \frac{1}{4} \text{Re}\{\alpha\} \vec{\nabla} |\vec{E}_0(\vec{r})|^2 \tag{3.4}$$

The time-averaged dissipative force is given as

$$\langle \vec{F}_{\text{d}}(\vec{r}) \rangle = \frac{1}{2} \vec{k}\, \text{Im}\{\alpha\} |\vec{E}_0(\vec{r})|^2 \tag{3.5}$$

Using the above expressions we calculate the optical forces on a gold nanorod along the propagation axis of the trap beam. The rod has the same dimensions as the rod in Fig 3.4. As a trapping beam we take a Gaussian beam with a 1.0 numerical aperture. We assume that the rod's long axis is

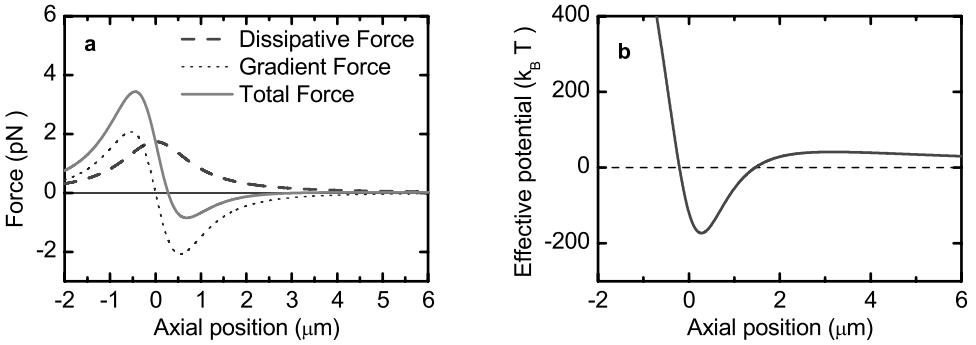

Figure 3.5: a) Calculated axial forces on a single gold nanorod, per Watt of optical power in the focus of a Gaussian beam of numerical aperture 1.0 and a wavelength 1064 nm. The nanorod polarizability is calculated in the electrostatic approximation, for a nanorod of volume of $2.5{\cdot}10^4$ nm^3 and aspect ratio 2.45 (longitudinal resonance wavelength in water 624 nm) in water. b) Corresponding effective axial potential, per Watt of optical power.

parallel to the field, and compute $\alpha_{\parallel}$ as the polarizability of the rod in the above equations. The results are plotted in Fig. 3.5a as functions of the position along the axis of the beam. We see that the axial equilibrium position (the position at which the total force on the rod is zero) is shifted by about 275 nm from the focus of the beam. For a beam with a numerical aperture of 1.2 this axial shift would reduce to about 150 nm. For lower NA the axial shift would be larger.

Figure 3.5b displays the effective potential experienced by the gold nanorod in Fig. 3.5a. This potential is an effective potential as the dissipative force does not derive from a true potential. The effective potential depth for the particle in a 1 W trapping beam is about 175 $k_{\mathrm{B}}T$ (with $T = 300\,\mathrm{K}$).

The trapping forces are proportional to the real part of the polarizability, with a positive real part leading to trapping at the intensity maximum of a focused beam. Larger values of the real part of the polarizability closer to the plasmon resonance lead to larger trapping forces. It would thus seem an advantage to use a trap laser with a wavelength close to the plasmon resonance, as long as it is on the long wavelength side of the half maximum of the resonance. However, this gain is more than compensated for by the larger imaginary part of the polarizability. Indeed, the imaginary part of the polarizability varies as a Lorentzian wing, whereas the real part follows a dispersion profile and decays much more slowly. The larger Im(α) leads to

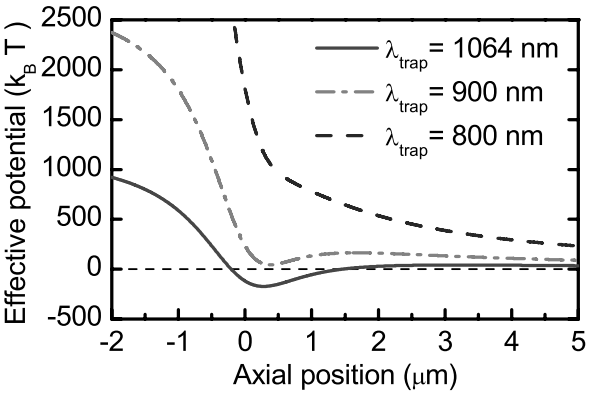

Figure 3.6: a) Calculated effective axial potentials, per Watt of optical power in the focus of Gaussian beam of 1.0 numerical aperture. The nanorod polarizability has the same parameters as the nanorod from figure 3.5.

a larger radiation pressure, pushing the particle out of the trap, as well as to more heating.

In Figure 3.6 we see the effective axial potentials that the same nanorod would experience for different wavelengths of the trapping laser. From the figure we see clearly the advantage of using a trap laser with a wavelength far in the red wing of the plasmon resonance. As the trapping wavelength approaches the resonance the effective potentials become less and less deep as the radiation pressure force starts to dominate the gradient force. For wavelengths below about 900 nm, stable trapping using a single beam gradient trap is no longer possible, at least for a numerical aperture of 1.0.

3.3.3 Optical torques

The anisotropic polarizability of gold nanorod leads to a trap potential that depends on the orientation of the nanorods with respect to the polarization of the trap laser

$$U(\theta) = -\frac{1}{4}\mathrm{Re}\left\{\Delta\alpha\right\} E_0^2 \cos^2\theta, \tag{3.6}$$

where θ is the angle between the polarization of the trap and the rod's long axes. $\mathrm{Re}\left\{\Delta\alpha\right\} = \mathrm{Re}\left\{\alpha_{\parallel} - \alpha_{\perp}\right\}$ is the difference between the real parts of the longitudinal and transverse polarizabilities of the nanorod at the trap wavelength. The potential energy is minimized when the long axis of the rod is parallel to the polarization of the trap, because $\alpha_{\mathrm{L}} > \alpha_{\mathrm{T}}$. For realistic intensi-

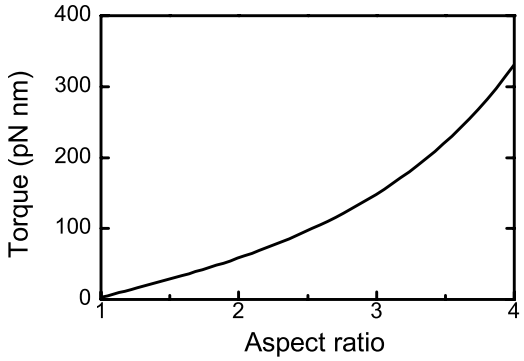

Figure 3.7: Maximum optical torque on a gold nanorod as function of aspect ratio, for a rod of constant volume. The torque is calculated according to Eq. 3.7, for typical parameters used in this thesis. The polarizability of the rod is calculated in the electrostatic approximation (Eq. 3.1) for a prolate gold spheroid of volume $2.5 \cdot 10^4\,\mathrm{nm}^3$ in water, in a beam with wavelength 1064 nm and with local intensity $2.4{\cdot}10^{11}\,\mathrm{W/m}^2$. The local intensity corresponds to an optical field amplitude $E_0 = 1.3 \cdot 10^7\,\mathrm{V/m}$ and, for typical experimental conditions in this thesis, to an optical power of about 80 mW at the focal plane. The maximum torque is proportional to the local intensity and, in the electrostatic approximation, to the volume of the ellipsoid.

ties of the trapping laser, the depth of orientational potential is several times the thermal energy. We thus expect that nanorods align in the optical trap.

To see the same property in a different way, we can evaluate the optical torque on the nanorod. The time-averaged optical torque on a dipole in an optical field is given as

$$\vec{T} = -\frac{1}{2}\kappa_{\mathrm{rot}} \sin(2\theta)\hat{kk} \tag{3.7}$$

where $\hat{kk}$ is a unit vector in the direction perpendicular to the rods long axis, and κ_{rot} is the rotational trap stiffness, given by

$$\kappa_{\mathrm{rot}} = \frac{1}{2}\mathrm{Re}\left\{\Delta\alpha\right\} E_0^2. \tag{3.8}$$

The maximum torque that is exerted on the nanorod is $T_0 = 0.5\kappa_{\mathrm{rot}}$. The torque is shown in Figure 3.7 as function of the rods aspect ratio.

Experimental Results

3.4 Thermal stability of trapped nanorods

Surface gold atoms are considerably more mobile than bulk ones. Surface diffusion leads to shape changes in gold nanoparticles, even at temperatures much lower than 1064°C, the melting temperature of bulk gold.[125] This phenomenon is called reshaping. Gold nanorods reshape into the thermodynamically more stable spherical shape, possibly with facets. While at room temperature gold nanorods in solution can be stable for several months to years, at a temperature of 250 °C rods reshape into spheres within 1 h.[125] During reshaping, the shape of the rod remains close to a spherically capped cylinder, and the particle aspect ratio can be deduced from the longitudinal plasmon wavelength, as for non-heated rods.[125]

As gold nanoparticles heat up in the optical trap due to absorption of the trap laser,[77,88,89] it is important to test for possible reshaping. We have studied the thermal reshaping of a sample of gold nanorods both on the ensemble level -by heating in an oven- and for single rods in the optical trap. The results on the ensemble of rods in the oven are shown in Fig. 3.8 (a) for a temperature of 95 °C. The sample had an average aspect ratio of 2.5, yielding a longitudinal plasmon resonance at 625 nm. The thermal reshaping leads to a blue shift of the longitudinal plasmon by about 3 nm in one hour, corresponding to a change in aspect ratio of about 1.5%. Fig. 3.8 (b) shows the plasmon resonance for 9 individual nanorods in the optical trap, as a function of the time spent in the trap. A first quick regime of blue shifting, seen in the inset for one of the rods, might be due to desorption of residual organic capping molecules (CTAB, PEG) due to the temperature change. This regime was followed by a very stable period, where the blue shift was limited to less than 1 nm in half an hour. Therefore, we conclude that reshaping was negligible for these nanorods, and that the temperature in the trap did not exceed 95°C. The results of Figure 3.8 show that single gold nanorods can be stably trapped with negligible reshaping, for periods of at least 0.5 h.

We have also observed thermal reshaping of trapped nanorods. Fig. 3.9(a) shows an example of a single nanorod that reshapes over time. This rod was first trapped at a low power, and a blue-shift is recorded upon increasing the trapping power. This blue-shift is attributed to reshaping. The process of reshaping in the trap is self-stabilizing: as the plasmon resonance shifts to the blue, the absorption at the trap laser wavelength decreases, the temperature of the rod decreases and the reshaping process is slowed down. As a result,

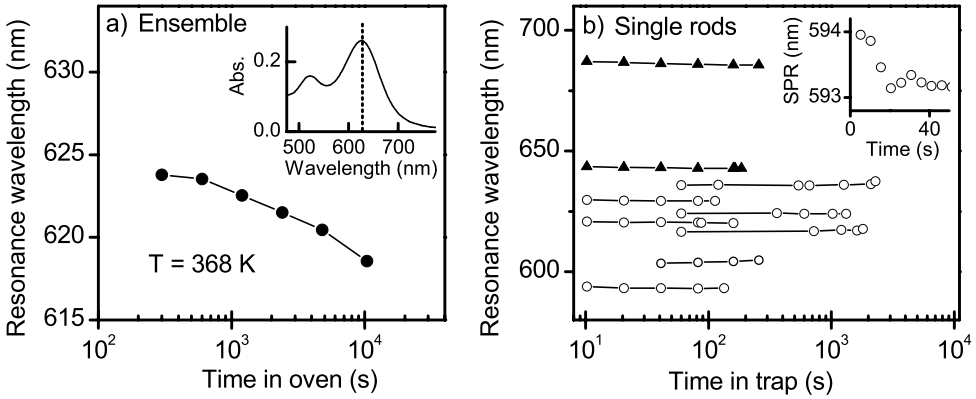

Figure 3.8: Thermal stability of gold nanorods (25 nm × 60 nm, PEG-coated). (a) Longitudinal plasmon resonance of an ensemble of gold nanorods in water, at different times after heating in a laboratory oven at 368 K (95 °C). Inset: Absorption spectrum of the ensemble before heating. The dotted line indicates the longitudinal plasmon resonance at 625 nm. (b) Longitudinal plasmon resonance of scattering spectra of 9 single gold nanorods in the optical trap, as a function of the time since they were first trapped. Inset: plasmon resonance SPR of one of the rods at short times. Trapping power at the focal plane was 60 to 80 mW (open circles) or 40 mW (solid triangles).

stable trapping at a given trap laser power will be limited to rods with an aspect ratio below a certain value. This behavior can be seen in Fig. 3.9 (b). Here we recorded the resonance wavelengths of about 20 nanorods in conditions where they were stably trapped, with plasmon shifts due to reshaping less then about 1 nm in 10 minutes. At the lowest trapping power, the average plasmon resonance is still close to the value measured on the ensemble. As the trapping power increases, only rods with shorter plasmon resonance wavelengths are stably trapped.

The results of Figures 3.8 and 3.9 show that gold nanorods can be stably trapped in three dimensions over extended periods of time (hours), but care must be taken to avoid thermal reshaping. In particular, trapping with a trap laser wavelength close to the plasmon resonance will cause a large absorption and lead to thermal reshaping of rods.

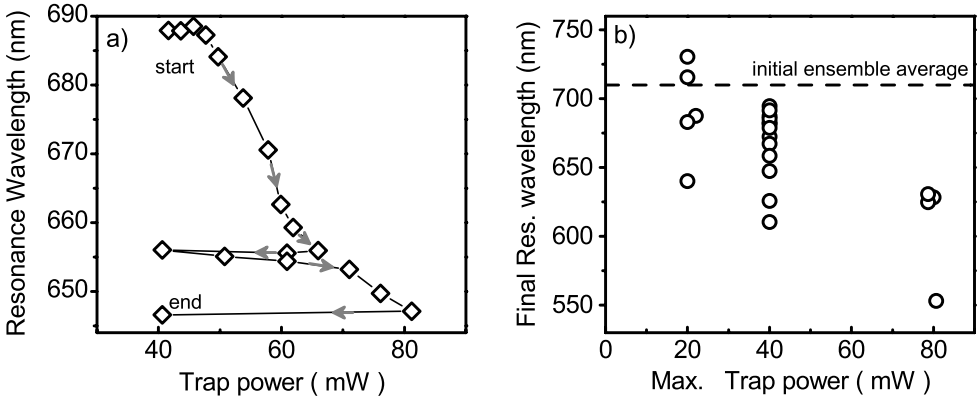

Figure 3.9: Thermal reshaping of single nanorods in the trap, (30 nm × 90 nm, PEG-coated). a) Trajectory of the longitudinal plasmon resonance of a single trapped nanorod as a function of trap power. The time interval between the start and the end of the trajectory was about 20 min. b) Final wavelength of the longitudinal plasmon resonance for a set of single gold nanorods in the trap, after reshaping. The data is plotted as a function of the maximum trap power that the individual rods were exposed to. The dashed line indicates the longitudinal plasmon resonance of the absorption spectrum of the ensemble. Indicated trap powers are at the focal plane.

3.5 Gold nanorods align with the trap polarization

As the scattering cross section of gold nanorods depends strongly on the polarization of the light relative to the long axis of the rod, alignment of the nanorods in the trap can be observed by analyzing the polarization dependence of the scattered light. Figure 3.10 (a) shows scattering spectra of a single gold nanorod, recorded with an analyzer in the detection path at various orientations with respect to the trap polarization. The incoming light from the thermal source is unpolarized. The spectrum recorded with the analyzer parallel to the trap polarization (0°) is much more intense than the spectrum recorded with the analyzer perpendicular. This observation shows that trapped gold nanorods align with their long axis parallel to the trap laser polarization. Fig. 3.10 (b) displays the polarization dependence of the intensity of the longitudinal plasmon over 360°. The dependence is well described by a squared cosine function, expected for the dipolar longitudinal plasmon resonance.

Due to thermal fluctuations, a trapped gold nanorod will undergo orientational fluctuation around the equilibrium orientation defined by the trap

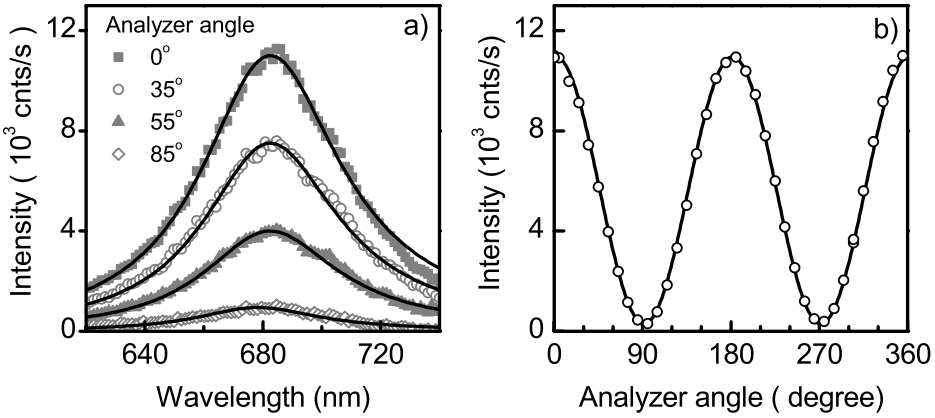

Figure 3.10: Alignment of a single gold nanorod in the trap observed by its polarization-dependent scattering spectrum (30 nm $\times$90 nm rod, PEG-coated). (a) Scattering spectra, recorded with unpolarized white light in excitation and an analyzer in the detection path. Spectra are shown for several orientations θ of the analyzer with respect to the trap polarization. Solid lines are Lorentzian fits, with resonance wavelength 682 nm and width 57 nm. (b) Maximum intensity of the longitudinal plasmon as a function of the orientation of the analyzer, obtained from the Lorentzian fit of the scattering spectrum. Solid line is a fit of a squared cosine plus offset.

polarization. The alignment of a rod in the trap will thus not be as perfect as would be observed for a nanorod immobilized on a solid substrate.

Fig. 3.11 (a) displays scattering spectra of a trapped nanorod, detected with an analyzer parallel or perpendicular to the trap polarization. The spectrum recorded with an analyzer perpendicular to the trap laser is much weaker. The spectrum shows residual intensity of the longitudinal plasmon around 630 nm and the transverse plasmon around 530 nm. Fig. 3.11 (b) shows that the polarization dependence of the intensities of the longitudinal and transverse plasmon is well described by a $\cos^2$ and a $\sin^2$ function, respectively, as expected.

The amplitude of the orientational fluctuation directly reflects the competition between the orientational trap depth and the thermal fluctuations. In Chapter 4 we will show how the polarization ratio can be used to quantify the optical torque acting on the trapped rod, by using Boltzmann statistics. A quantitative evaluation of the polarization intensity ratio rests on a polarization analysis of the light scattered by a single nanorod. The actual setup departs in two ways from the ideal situation of a nanorod precisely trapped at the focus of the linearly polarized excitation beam: i) the nanorod is displaced

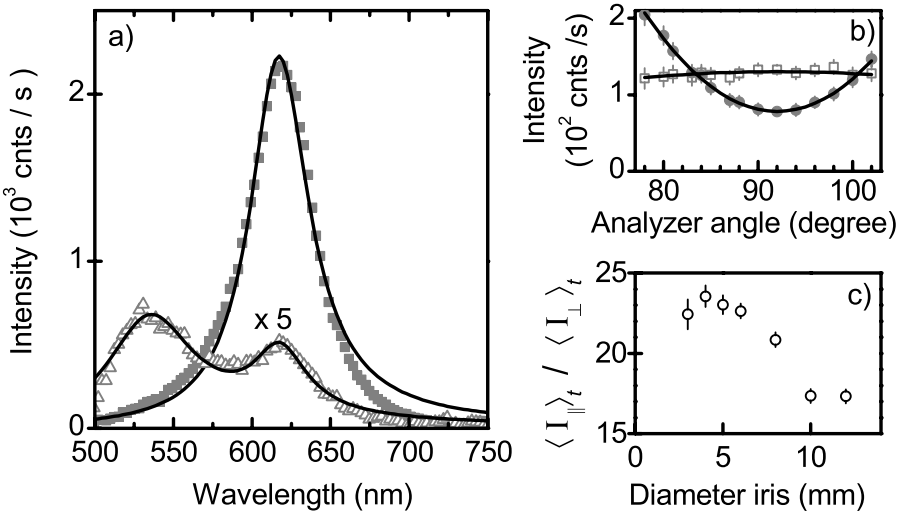

Figure 3.11: Polarization ratio of a single trapped nanorod, 25 nm × 60 nm. a) White light scattering spectra from a single trapped nanorod, with analyzer parallel (solid squares) or perpendicular (open triangles) to the trap polarization. Solid lines are Lorentzian fits (in frequency). The perpendicular spectrum is fitted with a sum of two Lorentzians. b) Spectral intensities recorded with the analyzer around the perpendicular orientation. Solid circles: Longitudinal resonance. Open squares: transverse resonance. c) Ratio $\langle I_\parallel \rangle_t / \langle I_\perp \rangle_t$ as a function of the diameter of the iris aperture in the detection path. Diameter of the objective back aperture is 11.5 mm.

from the focus and from the beam axis by thermal fluctuations. Therefore, it experiences polarization components in the longitudinal direction as well as along the perpendicular direction in the focal plane. Because of the rod's displacement, the scattered light will also be slightly depolarized with respect to the central position. ii) even when the rod lies at the center of the trap, the light scattered by the rod is collected with a large numerical aperture, which may lead to depolarization of the detected light. The magnitude of the latter effect can be minimized by limiting the solid angle of the detection.

Figure 3.11 (c) shows how the polarization ratio of light scattered by a trapped nanorod changes when an iris is placed in the detection path, as a function of the iris aperture. This ratio, which reaches 24 here for a strong alignment, clearly decreases for apertures larger than 6 mm, but keeps a constant value, within experimental error, for smaller apertures. For apertures less than 2 mm, the signal-to-noise ratio was too small to measure. For quantitative analysis of the polarization ratio (Chapter 4), the iris diameter was

fixed at 5 mm, a value for which depolarization in the detection is still negligible.

3.6 Characterization of trapping forces by position fluctuations

In Section 3.5 we have shown that single gold nanorods can be optically trapped in water for extended times, up to hours. This observation confirms that the potential depth of the trap is significantly larger than $k_B T$. This simple observation suffices for many of the applications of the trap discussed (or envisioned) in this thesis.

Applications that use optically trapped objects as a transducer of a known force or torque, require a quantitative knowledge of (the bottom of) the trap potential, and a measurement of the displacement (in position or angle) of the particle from the trap equilibrium position.

Here we characterize the optical potential by an analysis of the position fluctuations of the trapped particle, a method commonly applied in the literature for both microscopic dielectric and nanometric metallic particles.[67,75,126] In this method, the interference between the light scattered by the fluctuating particle and the transmitted trap beam is recorded on a quadrant photodiode (QPD) in the back focal plane of a collection objective. The motions of the particle in the trap can be recovered by an analysis of the intensity distribution of the beam. Specifically, a transversal displacement of the particle away from the trap center causes a transversely asymmetric intensity distribution, resulting in a voltage on the X or Y channels of the QPD, for which the signal is proportional to the difference in the intensity between the left/right, or up/down quadrants. A displacement of the particle in the longitudinal direction modifies the total collected intensity, represented by the sum of all quadrant signals.

The intensity distribution in the trap focus is approximately Gaussian in all three dimensions, resulting in a harmonic potential in the X, Y, and Z direction. The force on a trapped particle in each direction is then given by Hooke's law, with a spring constant (trap stiffness) κ. In each dimension, the Brownian motion of the trapped particle is described by a Langevin equation. For example, in the x-direction we have $m\ddot{x} = -\kappa_x x - \gamma_x \dot{x} + \mathcal{F}(T,t)$, where κ_x is the trap stiffness in the x-direction, γ_x is the corresponding friction coefficient, and $\mathcal{F}(T,t)$ is a term describing the white noise that results from the random collisions of the surrounding molecules with the particle.

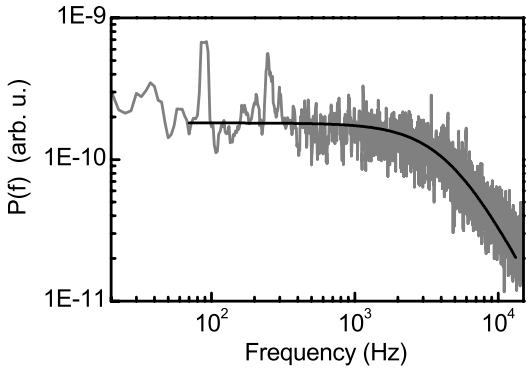

Figure 3.12: Power spectrum (in a transverse direction) of a single gold nanorod (sample average 30 nm diameter, 90 nm length, PEG coated), for transverse fluctuations of the rod. The black line is a fit of a Lorentzian with the corner frequency $f_c = 4.7$ kHz. The trapping power was 60 mW at the focal plane.

The inertial term can be neglected. The Fourier transform of the Langevin equation results in a Lorentzian power spectrum, with a corner frequency $f_c = \kappa/(2\pi\gamma)$.

Figure 3.12 displays the Fourier transform (power spectrum) of the transverse fluctuations of a single trapped gold nanorod. The spectrum is well fitted by a Lorentzian with a corner frequency $f_c = 4.7$ kHz.

The trap stiffness k can be obtained from the measured corner frequency if the friction coefficient of the trapped particle is known. For the friction coefficients of the rod, we use the expressions for a prolate spheroid derived by Perrin,[127] see Appendix D. Alternatively, we could use the expressions for a cylinder, derived in the limit for infinitely long cylinders, with a correction for their finite size.[128,129] The friction coefficients calculated by these two models for the gold nanorods in our experiment differ by less then about 20 % for rotational friction, and less then 2% for translation friction, see Appendix D. The interpretation of our experimental results is not sensitive to the model that is used, at least up to the accuracy obtained thus far. The advantage of the friction coefficients for ellipsoids is that the analytic expressions are valid for any aspect ratio. In contrast, the friction coefficients for cylinders are valid only for aspect ratios larger than 2.

More important than the geometric shape factor in the friction coefficient is the fact that all friction coefficients are proportional to the shear viscosity of the medium. Viscosity is a strongly temperature dependent parameter for many typically used liquids. For example, the viscosity of water at 90 °C is

more than a factor of 3 lower than at room temperature, see Appendix D. As the metal nanoparticle can heat up significantly in the trap, a first requirement therefore is to know the particle temperature, and the corresponding local viscosity. We can then describe the Brownian motion of the hot particle in an inhomogeneous temperature and viscosity profile, which will be discussed in Chapter 4.

3.7 Translational and rotational dynamics observed by photon correlation spectroscopy

To investigate the rotational dynamics of the rods in the trap we apply photon correlation spectroscopy on the polarized light scattered by the nanorods. Photon correlation spectroscopy has been introduced as a technique to characterize particles in optical traps by Bar-Ziv *et al.*[130] and Meller *et al.*,[131] for micron-sized dielectric particles. Photon correlation is a convenient technique to measure the rotational dynamics of nanoparticles as it provides access to a wide range of time scales in a single measurement, down to the nanosecond regime.[130] Whereas for a particle of 1 micron diameter rotational correlation times are on the order of seconds, the rotational correlation times of a 30 nm diameter particle is $3 \cdot 10^4$ times shorter, because the rotational friction coefficient scales as the particle volume. For these small particles, correlation times are on the order of microseconds or shorter, and are difficult to access with position-sensitive detectors.

Due to the optical anisotropy of gold nanorods, the rotational dynamics can be recorded with polarization-sensitive scattering measurements, as has been applied on freely diffusing ensembles of rods.[132,133] The rotational dynamics of weakly trapped gold nanorods have been measured by fluorescence correlation spectroscopy,[80] by averaging over many individual rods. To our knowledge, photon correlation has thus far not been applied to quantify the rotational and translational dynamics of single stably trapped particles (either metal or dielectric) with sizes below $\sim$100 nm.

3.7.1 Dynamics of a gold nanorods trapped in water

Here we provide autocorrelation functions measured on an optically trapped nanorod using a photon counting APD, with polarization-sensitive and polarization-insensitive detection. The result is shown in Fig. 3.13. The polarization-sensitive measurement is well fitted by a bi-exponential decay. The fast re-

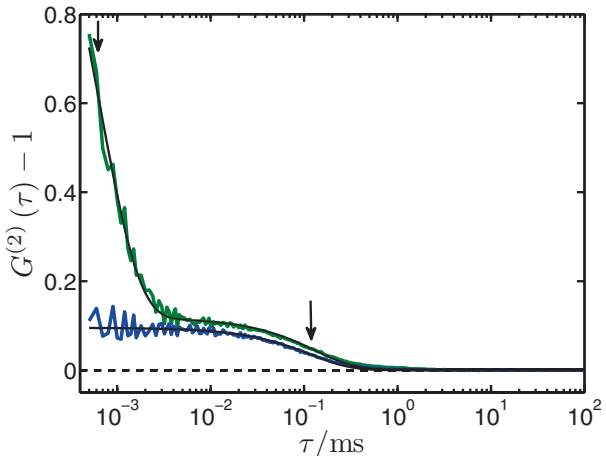

Figure 3.13: Autocorrelation functions of light from a HeNe laser, scattered by a single trapped gold nanorod in water. Green solid line: linearly polarized excitation parallel to the trap, with a detection analyzer perpendicular to the trap polarization. Blue solid line: Circularly polarized excitation, without analyzer in the detection. Solid black lines are a bi-exponential fit (characteristic times 0.64 $\pm$ 0.01 μs and 131 $\pm$ 0.6 μs, indicated by the arrows) and a single-exponential fit 118 $\pm$ 0.4 μs of the green and blue curves, respectively. Trapping power 80 mW, integration time 20 s.

laxation is due to rotational fluctuations of the rod in the trap. The slower relaxation is due to transverse and axial translational fluctuations in the trap. With the polarization-insensitive detection, only the slow translational part is seen. The correlation function is well fitted with a single exponential decay, with the same characteristic time as the one measured in the translational part of the autocorrelation function measured with the polarization-sensitive detection.

Dynamics of a gold nanorod trapped in a viscous glycerol mixture

Fig 3.14(a) displays the polarization-sensitive and polarization insensitive correlation functions on a single nanorod trapped in a viscous glycerol-water mixture. Here the rotational and translation relaxation times are slowed down. Whereas in water only the steep decrease of the rotational contrast could be detected, in glycerol the plateau of the rotational contrast can be clearly resolved.

Due to the much slower dynamics of the rod trapped in glycerol compared to pure water, in glycerol a fair number of photons ($\sim 10^2$) are collected

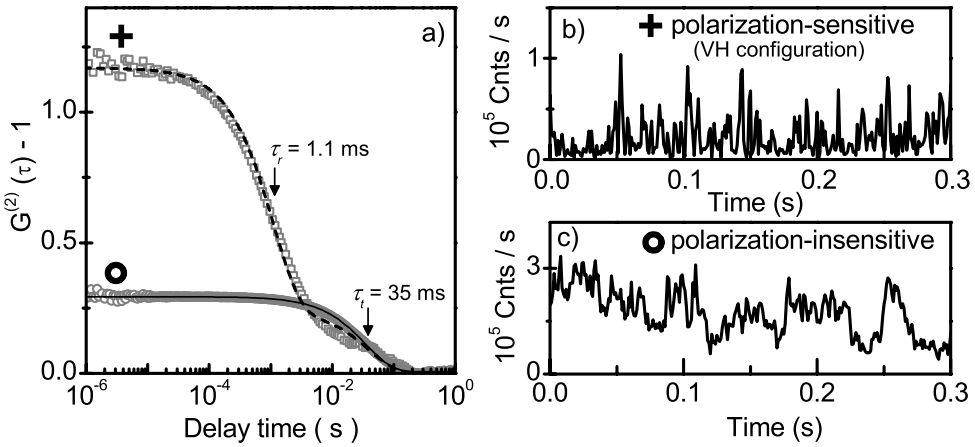

Figure 3.14: Translational and rotational dynamics of a single trapped gold nanorod in a viscous glycerol-water mixture (80% glycerol by volume). (a) Autocorrelation functions of light scattered by a trapped nanorod. Open gray squares: scattered light from a HeNe laser, with an analyzer in the perpendicular direction. Open gray circles: scattered white light from a Xe lamp, without analyzer. The solid (dotted) curves are (bi)-exponential fits with characteristic time(s) $\tau_t = 35 \pm 0.4$ ms ($\tau_t = 40 \pm 4$ ms and $\tau_r = 1.1 \pm 0.03$ ms). (b) Time trace of the scattered intensity of the HeNe light with analyzer in the perpendicular direction, directly showing the intensity fluctuations due to rotational fluctuations of the rod. (c) Time trace of scattered white light without analyzer, showing intensity fluctuations due to the rod's translational fluctuations. For the time traces, photon counts have been grouped in 1 ms time bins. Trapping power was 60 mW at the focal plane.

per rotational fluctuation time. The time traces of the scattered intensities in Fig 3.14 (b) and 3.14 (c) clearly show the intensity fluctuations due to rotational and translation fluctuations, respectively.

3.8 Conclusions

In this Chapter, we have shown that single nanorods of 25 nm nominal width and 60 nm nominal length (nominal aspect ratio 2.5) can be stably trapped in solution with an infrared single beam optical trap (1064 nm wavelength). We showed that the nanorods align along the polarization of the trap laser by time-averaged, polarization-sensitive white light scattering spectra. We measured the combined translational and rotational dynamics of the trapped nanorods by polarization-sensitive photon correlation spectroscopy. We have

investigated the thermal stability of the trapped gold nanorods, and found conditions under which rods can be trapped for more than half an hour without significant thermal reshaping. For rods with aspect ratios above about 3 significant reshaping was observed at the high end of the trapping powers used here, around 80 mW at the focal plane, corresponding to a local intensity of about $2{\cdot}10^{11}\,\mathrm{W/m^2}$. The lower thermal stability of the longer nanorods was attributed to the closer proximity of their longitudinal plasmon resonance to the trap laser wavelength, leading to larger absorption cross-sections and increased trap laser-induced heating. Our results show the promise of optically trapped gold nanorods as ultra-small trapping handles with control over both position and orientation. Additionally, our results demonstrate the important role of laser-induced heating of the rods. While conditions for stable trapping of single gold nanorods can be found, a careful in-situ determination of the thermal stability of the trapped nanorods is required.